Reliability assessment of steel truss railway bridges at ultimate limit state under combined loads

Mohammad Shihabuddin Khan[a,*], Colin Caprani[a], Roman Lenner[b], Miroslav Sýkora[b]

[a] *Monash University, Wellington road, Melbourne, 3168, VIC, Australia*
[b] *Czech Technical University, Šolínova 7, Prague, 166 08, Czechia, Czech Republic*

Abstract

The practical application of reliability assessments for large infrastructure, such as steel railway truss bridges, is impeded by many factors. These factors include the high dimensionality of the problem, the difficulty of integrating non-linear finite element analysis, and the general need for more information related to the probabilistic assessment of steel railway truss bridges. Additionally, most studies on steel railway truss bridges generally overlook performance at the ultimate limit state under combined actions and focus on fatigue assessment. Therefore, in this study, we propose a scalable and generalized framework for the probabilistic assessment of steel railway bridges using adjusted partial and combination factors. The framework addresses many practical challenges associated with the probabilistic modelling for steel railway truss bridges, such as load and resistance uncertainties, horizontal forces such as braking and nosing, wind loads and railway line operator decisions,

*Corresponding author
Email addresses: shihab.khan@monash.edu (Mohammad Shihabuddin Khan), colin.caprani@monash.edu (Colin Caprani), roman.lenner@fsv.cvut.cz (Roman Lenner), miroslav.sykora@cvut.cz (Miroslav Sýkora)

[1]

load effect combinations and correlations, and factor adjustment. The framework is demonstrated for assessing two longitudinal girders of a single-span 60 m steel railway truss bridge. Relevant input data and results are provided as a dataset for complete ease of reproducibility of the results. Notably, it is found that nosing loads are critical for the girders due to the induced large minor axis bending moments. Furthermore, some potential ways of reducing the dimensionality of the resulting factors are explored, which significantly impacts the resulting design's efficiency.
Keywords: reliability assessment, code calibration, LRFD calibration, railway bridge, steel truss bridge, partial safety factors

---

1. Introduction

The performance inadequacy of degrading infrastructure is a widely recognized problem that affects infrastructure globally. ASCE [1] noted that approximately 46 000 (or 7.5%) of all American bridges are structurally deficient, with a bridge repair backlog estimates exceeding $125 billion. Similarly, Bień et al. [2] report that close to 35% of all European railway bridge stock is over 100 years old. Furthermore, around 36% of all European railway bridges are composed of steel [2]. These degrading steel railway bridges are subject to higher traffic volumes, travelling more frequently and at higher speeds. Therefore, an accurate safety assessment of these deficient railway bridges is urgently required.

Typically, engineers adopt semi-probabilistic assessment methods for bridges [3, 4]. However, these methods fail to capture the full range of underlying uncertainties within the load and resistance variables. Therefore, probabilistic approaches are increasingly favoured, as they can help uncover the reserve structure capacity of built infrastructure stemming from a conservative design process [5, 6, 7].

Various studies have noted the benefits of reliability assessment for assessing old railway bridges [8]. Casas et al. [9] recommends an "enhanced assessment" including non-linear finite element analysis (FEA) coupled with reliability assessment as the ideal assessment strategy. Practically, "enhanced assessments" for steel railway truss bridges are impeded by three major factors.

Firstly, most studies overlook the performance of the bridges at the ultimate limit state (ULS) and focus on fatigue performance [10, 11, 12]. A few studies have considered ULS though: O'Connor et al. [13] conducted a simplified reliability of riveted connections of a steel bridge with a single variable load using a generic probabilistic model; Nadolski et al. [8] presented a simplified reliability analysis of the bridge with just a single variable load, and; Žitný et al. [14] analyzed the reliability of the steel truss bridge at the ULS of equilibrium. However, the findings of these works are not general, and cannot be considered where uncertainties such as wind-on-train load, resistance characteristics, resistance model uncertainty, dynamic and horizontal effects of traffic load and thermal load effects are significant. Therefore, the performance of steel girders under combined actions, such as train, braking and nosing forces, requires more investigation.

Secondly, the integration of non-linear FEA and reliability assessment models is impeded by the scale of the assessment problem in three aspects: (i) the large number of structural elements constituting the truss bridge; (ii) multiple simultaneously acting load cases and consequent effects, and; (iii) very high computational costs of FEA and reliability assessment. While some studies have explored metamodelling, and simplified methods for assessment [15], their applicability and accuracy are limited by the numerous simplifying modelling assumptions.

Finally, while Bień et al. [2] and Casas et al. [9] provide guidelines for the probabilistic assessment of railway bridges, many essential aspects specific to steel railway truss bridges lack detailed exposition. In particular, the model errors, uncertainties within horizontal loads, and load effect correlations and combinations have been little considered.

To address the aforementioned problems, in this study, the authors present a scalable and generalized framework for the probabilistic assessment of steel railway bridges using adjusted partial and combination factors. This framework leverages the strengths of linear-elastic analysis methods and reliability assessments to develop adjusted safety factors for application in semi-probabilistic non-linear structural analysis assessments. Relevant input data and results are provided as a dataset for complete ease of reproducibility of the results [16]. The study presents the framework in Section 2. Section 3 discusses some modelling challenges, complexities, and potential solutions. The study applies the framework on an existing steel railway bridge in Section 4. Section 5 concludes with some remarks and recommendations for further research.

2. Framework for reliability assessment of steel railway truss bridges

2.1. Overview

The overall flowchart of the proposed framework is illustrated in Figure 1. The methodology is divided into four stages with six mutually cooperating analysis 'modules', as explained below.

2.2. Stage I: initial analysis and database generation

This stage is used to reduce the scale of the assessment problem while maintaining the accuracy of the overall assessment framework. The objectives of this stage are to: (i) identify a set of critical members for probabilistic assessment; (ii) generate a database of load effects acting on the critical members, and; (iii) generate a database of relevant structural and material properties for all critical members. A linear elastic analysis model helps achieve all three objectives of this stage, although in some cases, a dedicated structural properties model may be required.

Linear elastic 3D finite element (FE) frame models can analyze truss bridges more quickly than non-linear FE shell models, to estimate the load effect. The relevant design code provisions specify the magnitude and application of time-invariant and time-varying loads, for example, in Australia this is [17]. The maximum varying load effect, such as that for wind on trains, horizontal nosing, and vertical train loads, can be estimated using influence lines generated from the analysis model. Furthermore, such frame models facilitate investigating alternative load paths stemming from structural degradation. Based on the resulting load effects, the most critical structural members are identified for a detailed probabilistic assessment.

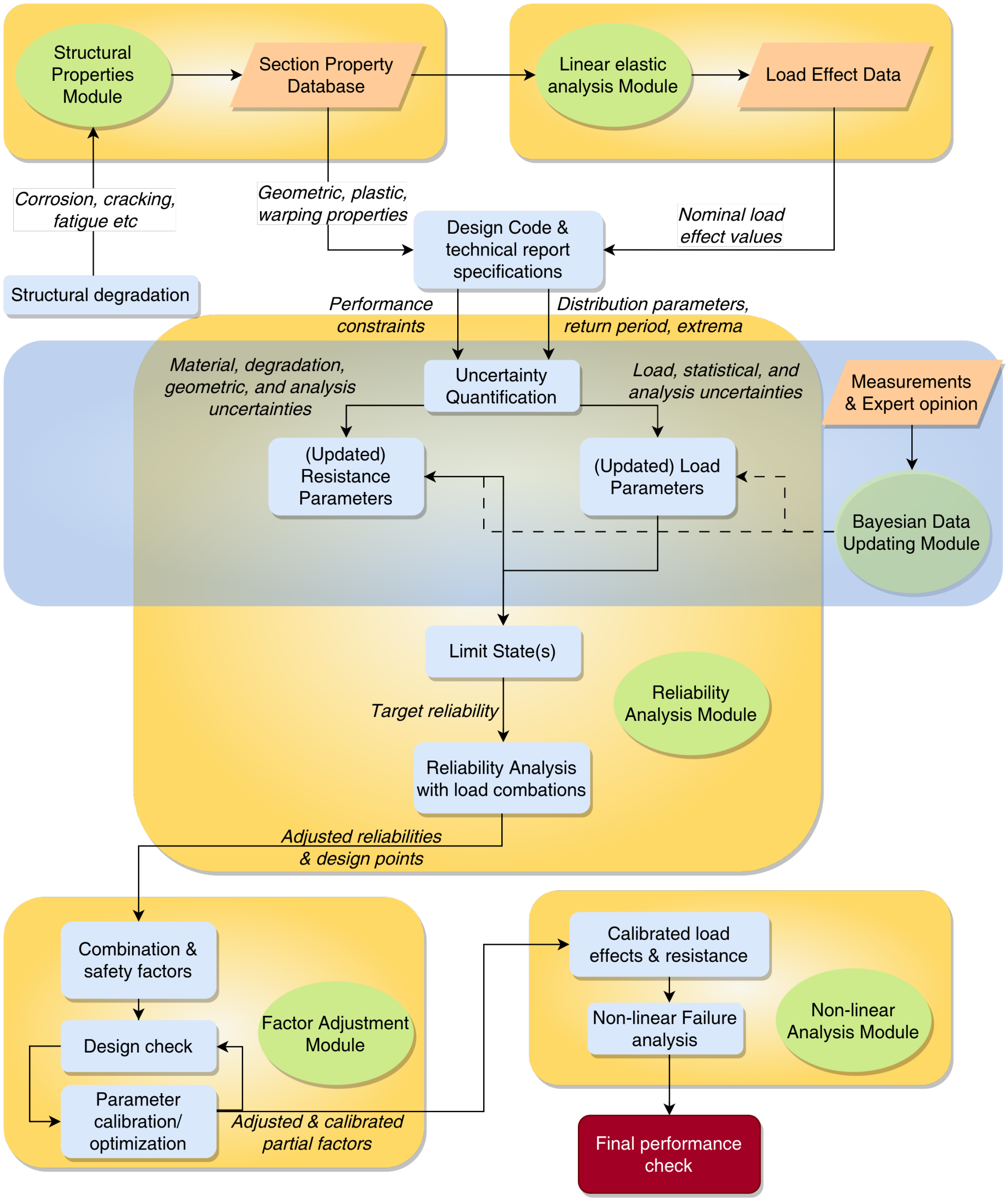

Figure 1: A conceptual illustration of the probabilistic assessment framework.

Furthermore, the critical elements' section properties, such as plastic section modulus, can also be generated. These section properties are required for estimating the resistance of the structural member quickly as per a structural design standard. They should also account for any reported structural degradation, such as corrosion.

2.3. Stage II: uncertainty quantification

The objectives of this stage are to: (i) establish the statistical properties of the resistance and load parameters; (ii) incorporate measurement data/expert opinion for updating the statistical properties, and; (iii) establish the relevant limit states and load combinations for reliability analysis.

An essential source for uncertainty quantification is the structural design code. It typically specifies the following relevant information: (i) the return period of load actions for the nominal value [18]; (ii) the performance requirements on the sections for identifying the relevant limit state(s), and; (iii) the interrelationship between various load effects for load combinations and correlations.

2.3.1. Statistical properties

Generally, the parameters of a statistical distribution can be established by specifying the X_k is the nominal or characteristic value (e.g. the 95-percentile or loading for a return period specified by the design code), bias (λ), and Coefficient of Variation (CoV), as:

$$\lambda = \frac{\mu_X}{X_k}, \tag{1}$$

and

$$CoV = \frac{\sigma_X}{\mu_X}, \tag{2}$$

where μ is the mean, and σ is the standard deviation of the distribution.

The design code, site-specific information, and other technical guidance can be used to establish these parameters [19, 20, 21]. The maximum load effects from the analysis model can be taken as the nominal value. Similarly, the section properties database can be used with design code and other specifications to establish the nominal value of the resistance variables.

2.3.2. Site-specific information

Bayesian statistics provides a formal mathematical framework to update statistical distributions of prior information by utilizing site-specific information [22]. Such information can be available through limited in-situ measurements (such as historical traffic load data, material properties, wind drag coefficient, and structural degradation) and expert opinion. This information acquisition can incur high costs and, therefore, it should be justified by using Bayesian preposterior analysis to quantify the potential monetary benefits of such information [23].

2.3.3. Load combinations for reliability analyses

The probability of simultaneous occurrence of multiple extreme loads is very low, thereby necessitating proper probaility modelling of load combinations. Keeping the focus on stationary situations and ultimate limit states only, a few studies and documents [21, 24, 25, 26, 27] applied:

1. the Ferry Borges-Castanheta (FBC) processes — sequences of indepen-

dent, identically distributed random variables, each acting over a given (deterministic) time interval;

2. various types of intermittent or non-intermittent renewal process, and;
3. outcrossing approach for random continuous process.

An approximate method is Turkstra's rule [28], which considers a dominant action at its maximum at time t and non-dominant action(s) at their expected point-in-time value. When the chosen reference basis is annual and daily maximum, it can be generalized for any number of load effects S_i as:

$$S_{max} = \max_{i}\left[\max_{year} S_i + \sum_{j \neq i} \max_{day} S_j\right] \tag{3}$$

In comparison to the aforementioned higher-level approaches, Turkstra's rule has been found to provide reasonably accurate in many situations [29] and has been thus adopted as the basis for load combination rules in codes of practice. Its application requires fewer input data, such as information about distributions for short reference periods, seasonal variability of climatic and traffic loads, and dependencies between loads. Nevertheless, more detailed load combination analysis may be needed in case of several equally critical variable load effects, large number of loads, large failure probabilities (e.g. for serviceability), and strongly non-stationary cases.

2.3.4. Maximum and parent Distribution Statistics

In many cases, explicit statistical data for both, parent and maximum distributions, may not be available. Under such circumstances, extreme value theory can be utilized for inferring the statistics of either the parent or the maximum distribution. For some distribution families, such as the Gumbel, the stability postulate can be used to determine the parameters of the parent distribution analytically from its (n-maximum) using linear transformation [30].

2.4. Stage III: adjustment and calibration of factors

The primary objectives of this stage are: (i) adjustment of the partial safety and combination factors relative to their design code stipulated values based on a chosen target reliability index; (ii) calibration or optimization of the factors for a family or population of structural members, and; (iii) check of calibrated factors using a forward reliability analysis of calibrated factor-based design. These calibrated factors are then employed in a final performance check of the section.

2.4.1. Factor adjustment

Factors can be adjusted using expert judgement, design value method, or reliability optimization [31]. Factor adjustment using optimization involves adjusting the design parameter z in the limit state function (LSF) such that the probability of failure corresponds to that of the target reliability index (β_T) and identifying the most probable failure point, i.e. the design point [32, 33]. For example, consider the LSF $G\left(X\right)$:

$$G(X) = zR - Q_1 - Q_2, \tag{4}$$

where z is a scalar design parameter, R is the resistance variable, and Q_i are the transient loads.

This problem considers two load cases. In first, Q_1 has the maximum distribution for a chosen reference period (e.g. annual maximum), and Q_2 has a point-in-time distribution for a chosen basis (e.g. daily maximum). In second, the converse situation exists. Therefore, once calibrated, $z = z^*$ such that:

$$-\Phi^{-1}\left[\mathbb{P}\left[G(z^*) \leq 0\right]\right] = \beta_T \tag{5}$$

The design point at β_T for the two load cases can be represented as

$$X^*_{\beta_T} = \begin{bmatrix} z_1 \; R_1^* & S_{11}^* & S_{12}^* \\ z_2 \; R_2^* & S_{21}^* & S_{22}^* \end{bmatrix} \tag{6}$$

The objective of a typical semi-probabilistic design is to ensure that the design resistance R_d is greater than the design loads $S_{d,i}$, i.e.

$$R_d \geq \sum_i S_{d,i} \tag{7}$$

where the design load and resistance variables are given by,

$$\begin{aligned} S_{d,i} =& \psi_i \gamma_i \; S_{k,i} \\ R_d =& z \; \phi \; R_k \end{aligned} \tag{8}$$

where $S_{k,i}$ is the characteristic value of the ith load, R_k is the characteristic value of the resistance, ϕ is the resistance factor, ψ_i are the combination factors, and γ_i are the load factors. Therefore, by comparing the corresponding terms in Equations (6) to (8), the estimates of ϕ, ψ, and γ adjusted to β_T can be obtained.

2.4.2. Factor calibration

The aforementioned method of estimating factors yields unique values of partial load factors for the time-varying load effects, and estimates of partial load factors for time-invariant load effects, partial resistance factors, and combination factors for time-varying load effects differing per load case. In cases where the number of critical sections under consideration is large, this will result in a very high volume of data generation, thus complicating assessment for the asset manager. Therefore, these adjusted partial factors can be further calibrated (or optimized) for all or a family of sections to obtain an optimized set of partial factors [8].

2.4.3. Design check

Such calibration of partial factors and the design check are conducted iteratively, as shown in Figure 1. The design check uses the adjusted (or calibrated) partial and combination factors to estimate the corresponding scalar design parameter z using Equations (7) and (8). Then, based on the estimated z, a forward reliability analysis is conducted to estimate the achieved (design) reliability. This process mimics the design process and, therefore, is termed a design check. For any valid set of partial and combination factors for an assessment problem, for the assessment of a single structure, the obtained reliability must be greater than β_T in all load combinations. Any conservative enveloping of adjusted factors (e.g., taking the maximum factor for a specific load effect type across a population of sections) would increase the design reliabilities greater than β_T.

2.5. Stage IV: final performance check

Using the adjusted and calibrated partial factors, the calibrated load effects acting at a section can be estimated. These calibrated load effects can be applied to a non-linear analysis model of the section, and corresponding resistance at failure can be estimated. Therefore, utilizing Equation (7), the final performance check of the section using the adjusted and calibrated partial and combination factors at β_T is obtained. Such a targeted probabilistic assessment helps the asset owner avoid unnecessary conservatism stemming from the design code stipulated partial and combination factors, while retaining the simplicity of a rating factor check.

3. Modelling and assessment challenges and considerations for steel railway truss bridges

The framework proposed in Section 2 and Figure 1 presents numerous modelling considerations, complexities, and challenges for the asset owner which are discussed below.

3.1. Load effect and resistance uncertainties

3.1.1. Model uncertainties

In scientific models, some uncertainties are reduced by repeated observations, i.e. epistemic uncertainty, and others remain due to the stochastic nature of the phenomenon, i.e. aleatory, [34]. Repeated observations indicate less uncertainty and, hence, a narrower probability distribution. These uncertainties cannot be quantified separately in many practical structural engineering scenarios. Under such circumstances, uncertainties characterizing the FE model (ω_{S_f}) and the analytical model of structural "strength" (ω_{S_m}) can be considered.

Consider a steel section under the combined action of major axis bending moment M_z, minor axis bending moment M_y, and axial force N. The ULS considering structural uncertainties can be written as,

$$G = 1 - \omega_{S_m} \left[\frac{\omega_{S_f}\ M_z}{\omega_R\ M_{z_R}} + \frac{\omega_{S_f}\ M_y}{\omega_R\ M_{y_R}} + \frac{\omega_{S_f}\ N}{\omega_R\ N_R} \right] \tag{9}$$

where M_{z_R} is the nominal section major bending capacity, M_{y_R} is the nominal section minor bending capacity, and N_R is the axial strength of the section. ω_{S_m} accounts for the structural strength model uncertainty under the combined actions, i.e. the failure surface. The phenomenon's complexity results in various approaches in engineering practice. For example, EN 1993 1-1 [35] provides two alternative methods for evaluating the performance under combined actions. Similarly, AS 4100 [36], AS 5100.6 [37] specify a power function with reduced section bending capacities for compact doubly symmetric sections. Therefore, ω_{S_m} represents a significant uncertainty that must be incorporated within the LSF.

The uncertainty within the FEA model, ω_{S_f}, stems from various sources. Firstly, any simplifications of the numerical model describing the development of internal forces, such as the idealization of supports, spatial variability considerations, and composite actions of structural members, add uncertainties. Secondly, there exist uncertainties particularly relevant for steel railway bridges, such as the behaviour of joints, supports, initial imperfections, behaviour of material, section and members under different load levels and related changes in stiffness, and load redistribution. Material and physical non-linearity can significantly affect load redistribution and resulting load effects on steel structures. The stiffness of joints or the stiffness of secondary elements (such as bracing) in the actual structure can deviate from that assumed in the structural analysis model. Thirdly, the numerical algorithms for FEA solutions can impart errors. Finally, the uncertainty can vary per load effect magnitude. For example, bolted connections work linearly at low load levels while at higher load levels slips and deformations increase uncertainty [8].

In cases where these uncertainties cannot be defined explicitly, a combined uncertainty model can be considered that accounts for both ω_{S_f} and ω_{S_m} as,

$$G = \omega_R - \omega_S \left[\frac{M_z}{M_{z_R}} + \frac{M_y}{M_{y_R}} + \frac{N}{N_R} \right] \tag{10}$$

3.1.2. Statistical models for load uncertainties

There exist few studies that guide modelling load uncertainties. In particular, explicit statistical models for ω_{S_m} are not readily available. Cajot et al. [38] indicates a mean ranging between $1.28 - 1.58$ and a CoV of 0.10, approximately, for the EN 1993 strength model.

Some existing studies offer guidance on modelling ω_{S_f}. JCSS [39] offers models for the load effect calculation and resistance models for steel and concrete. These models are enhanced by Braml et al. [40] considering work done by Faber [41] and Hansen [42] leading to adjusted CoV for the resistance. Scholten et al. [43] lists case-specific uncertainties for variable loading based on the confidence level in modelling of a structural system, geometric proper-

Table 1: Statistical models for load uncertainty, ω_S.

Type	Distribution	Mean	CoV	Ref
ω_{S_m} for EN 1993 1-1 [35]	—	1.28-1.58	0.10	[38]
ω_{S_f} for axial forces	Lognormal	1.0	0.05	[39]
ω_{S_f} for beam bending	Lognormal	1.0	0.10	[39]
ω_{S_f} for plate bending	Lognormal	1.0	0.20	[39]
ω_{S_f}	—	1.0	0.10-0.20	[43]
ω_{S_f} for permanent loads	—	1.0	0.07	[45]
ω_{S_f} for traffic loads	—	1.0	0.10	[45]

ties and crossing mode. James [44] discusses model uncertainties for various limit states of railway concrete bridges, and notes that for the train loading, model uncertainty is already included in the uncertainty of the static load; hence omitted in the reliability calculations.

Considering a standard numerical finite element model, model uncertainty statistics are summarized in Table 1. JCSS [39] specifies models for load effects on beams and plates. Danish practice [43] specifies models based on low/high load confidence level. These values partially align with the recommendation of Steenbergen and Vrouwenvelder [45].

3.1.3. Statistical models for resistance uncertainties

For members in compression, the resistance models address the complex situation where [46]:

1. Depending on the shape of a cross-section, steel members are susceptible to torsional deformations;
2. One buckling mode dominates – commonly, spatial buckling deforma-

Table 2: Statistical models for resistance uncertainty, ω_R.

Type	Distribution	Mean	Bias	CoV	Ref
Bending and shear	Lognormal	1.0	—	0.05	[39]
Axial compression	—	—	1.15	0.10	[47]
Bending	—	—	1.10-1.15	0.08-0.10	[47]
Bending	—	1.1-1.3	—	0.04-0.07	[38]
Axial	—	1.1	—	0.045	[38]

tion of such members is divided into the two buckling modes about the strong and weak axis, and;

3. End and intermediate lateral restraints affect buckling lengths.

Design code stipulations suggest that member compactness has a crucial bearing on estimated structural capacity [36, 35]. The differing theoretical models suggest difficulty of capturing the various mechanisms contributing to the overall resistance of steel members. Further, statistical information on related resistance model uncertainties, ω_R, is scarce. These uncertainties will depend upon the dominating failure mode.

Table 2 summarizes some statistical models for steel resistance uncertainties from different sources. Note that applying a non-linear FE method will reduce resistance model uncertainty in cases when a dominating failure mechanism is difficult to identify. Therefore, reliability-adjusted and calibrated safety and combination factors will significantly benefit a non-linear FE analysis.

3.2. Horizontal force modelling and uncertainties

Braking and nosing forces, acting horizontally at the top of the rails, are often important in reliability verifications of railway bridges. Their effects depend on the speed and type of the train, track curves, and geometry of the bridge deck. Generally, no dynamic amplification is considered. Braking forces act in the longitudinal direction along the track. They can be considered as uniformly distributed over the corresponding influence length. In contrast, nosing forces are concentrated, acting perpendicular to the centre line of a straight or curved track.

The major considerations associated with these horizontal forces for reliability assessment of railway bridges are: (i) scarce statistical models for horizontal force uncertainties; (ii) low frequency of accidental braking events; (iii) potential high conservatism in load models for assessment, and; (iv) their interrelationships and correlations.

Detailed statistical models for braking and nosing loads are scarce. Measurements covering the effects of representative types of trains can substantially decrease design horizontal forces for purposes of assessment.

3.2.1. Braking force

A comparison of the Eurocode, UIC, and several national braking force models (Austrian, Czech, German, Swedish, and Swiss) with in-situ measurements indicates general overestimation of load effects by the code models [48]. Furthermore, braking at high speeds ("accidental braking" in some unexpected extreme situations) on bridges is rare. Czech railway operator data analysis reveals that about one accident in 10 years can occur in one kilometre of a track [49]. Additionally, the frequency of such events on bridges is much lower than that in open terrain because accidental braking is usually caused by some obstacles on the track like fallen trees. Therefore, the low measured forces and low accidental braking frequency on a bridge suggest a low mean braking force relative to the design code load effect.

There needs to be more information on the uncertainties within the braking load models of various design codes such as EN 1991-2 [50] and AS 5100.2 [17]. Without detailed statistical models, the uncertainties within braking force estimates can be considered the same as those for vertical train loads due to their close phenomenological relationship. Note that traction forces are generally ignored in reliability analyses as they commonly lead to lower load effects than braking forces [49].

3.2.2. Nosing force

While the general ambiguity behind the exact phenomenological basis of nosing forces indicates its consideration as a notional load representative of various phenomena, these forces are usually associated with the rail hunting or lateral track shifting forces exerted by each train wheelset on the rails and ballast. AS 7508 [51] suggests that they result from the unbalanced lateral acceleration and can be especially significant on curves with high cant deficiency at high speeds.

UIC Code: 776-1 [52], which forms the basis of most EN 1991-2 [50] provisions for railway bridges, recommends a characteristic value of 100 kN for nosing loads. On the other hand, AS 5100.2 [17] also recommends 100 kN but with provisions to scale the characteristic value in proportion with the specified design traffic load. AS 7508 [51] recommends a maximum value of lateral track shifting forces ($S_{\mathrm{LTSF,\,max}}$) as a function of the vertical axle loads as:

$$S_{\text{LTSF, max}} = 0.85 \left(10 + \frac{A}{3}\right) \tag{11}$$

where A is the vertical axle load in kN.

These design values seem conservative since the railway operators do not experience many related failures. Georgiev et al. [53] indicates that the Eurocode nosing forces are overestimated by a factor of 4 times for freight trains at speeds up to 80 km/h. Additionally, passenger trains induce even lower nosing forces. Furthermore, AS 7508.1 [54] suggests an inversely correlated relationship between vertical axle loads and horizontal nosing loads due to increased frictional resistance for heavier axles. Therefore, measurements of the effects of representative trains can substantiate decreasing design nosing forces, particularly for railway bridge assessment. Detailed statistical models for nosing loads are unavailable at present. Without any established statistical model for nosing loads, they can be considered the same as that for vertical train loads.

3.3. Wind load effect and operator decisions

3.3.1. Operator decisions

The probability of simultaneous strong wind and heavy trains crossing the bridge can be estimated from the databases for wind speeds and traffic flows. However, railway-line operators usually interrupt the railway traffic when forecasted wind speed exceeds a specified threshold to ensure safety and minimize rail derailment. For instance, in Australia many railway operators restrict train passage at $v \geq 28$m/s; this threshold is adopted in the case study in Section 4. In Germany, Deutsche Bahn AG [55] introduces a threshold of 30 m/s. Fujii et al. [56] addressed traffic operation control under high wind speeds in Japan.

Wind speed operating thresholds reduce the probability of extreme wind-on-train load effects. The consequent impact on reliability is significant but difficult to capture [14]. Probabilistic approaches, such as Bayesian Networks, can be adopted to develop the marginal distribution of the wind-on-train load effect. Such a strategy would integrate the uncertainties from the independent variables, such as the wind speed, forecasting model, and operator decisions. Moreover, such an imperfect decision-making process entails many uncertainties that must be captured within these probabilistic models.

3.3.2. Wind load direction reversal

While modelling wind loads, the structural members are analyzed for one or more possible directions of the winds based on the anticipated most adverse outcomes. The assessment results for all wind load directions considered can be then enveloped to establish the most critical wind direction case specific to each member. However, within each assessment scenario, the direction of the wind loads is considered to be fixed and unchanging.

In cases when the annual maximum wind load distribution has a real-valued support, such as the Gumbel distribution, it is possible that some probability content of the inferred parent distribution can spill over to the opposite, negative or positive, domain. In physical terms, such a change of sign indicates a change of wind load direction within an assessment scenario and, therefore, it must be restricted.

Such a restriction on the wind load direction can be done in the following ways. Firstly, if suitable, a strictly positive probability distribution (such as exponential distribution) can be adopted. When the load effect is negative as per the chosen sign convention (e.g. sagging is positive and hogging is negative), the nature of the load effect can be captured by encoding a -1 multiplier with the load effect within the LSF. Alternatively, actual statistical data regarding the wind load effects can be developed instead of adopting extreme value theory for inferring the distribution parameters. In any case, such a wind load direction reversal must be restricted, but it must be done so carefully so as not to introduce artificical truncated distributions into the reliability assessment. Otherwise, the reliability results will erroneously magnify (or diminish) the impact of wind loads on the structural member.

3.4. Load effect combinations and correlations

3.4.1. Load combinations specification

For ULS, most structural design codes specify load cases a combination between the permanent effects (including prestressing) and transient load effects. In contrast with BS EN 1990 [57], AS 5100.2 [17] specifies the load combination factor for the non-dominating transient load effects as zero but accounts for the rare probability of joint simultaneous occurrence of various transient loads by adjusting the characteristic value of some accompanying loads in various subclauses.

Permanent load effects, such as Dead Load (DL), Superimposed Dead Load (SDL), and Track Load (TL), retain their distributions throughout the reliability assessment. For steel railway bridge assessment at ULS, it is important to consider load combinations:

Table 3: Load combinations considered in the study.

Label	T & BF	NO	WB & WT
C1: T max	Max	Parent	Parent
C2: N max	Parent	Max	Parent
C3: W max	Parent	Parent	Max

- *C1: T max*: annual maximum of Train Load (T) and Braking Force (BF) is combined with daily values of Nosing Load (NO), Wind on Bridge (WB), and Wind on Train (WT); the latter being truncated with the upper bound at the threshold of wind speed for traffic interruption (Section 3.3.1).

- *C2: N max*: annual maxima of NO are combined with daily values of T, BF, WB, and WT.

- *C3: W max*: annual maximum of wind pressure is applied as follows:

    1. WB and WT is combined with daily values of T, BF, and T for wind speeds below the threshold,
    2. for wind speeds exceeding the threshold, WB is considered only.

For this study, additional numerical analyses revealed a good match between reliability indices based on Turkstra's rule and FBC processes. Further, when point-in-time (parent) distributions of variable loads are based on weekly maxima, slightly conservative estimates are obtained. On the other hand, consideration of monthly maxima for accompanying variable loads leads to conservative estimates. Therefore, Turkstra's rule is deemed appropriate for this study.

3.4.2. Load correlations specification

Correlations are particularly important for: (i) the correlations between load effects for a particular load type (e.g. major-axis bending and minor-axis bending of a given load type), and; (ii) correlations between various loads themselves (e.g. vertical train loads and nosing). Based on the phenomenological inter-relationships between various loads, Tables 4 and 5 present a qualitative recommendation on the degree of correlation for steel railway bridge assessment. These qualitative correlation intensities range from very low to perfect correlation.

Table 4: Qualitative correlation between bending moment and axial forces load effects for a given load case.

	M_{z_S}	M_{y_S}	N_S
M_{z_S}	Full	Very High	High
M_{y_S}	Very High	Full	High
N_S	High	High	Full

Table 5: Qualitative correlation between bending moment and axial forces load effects for a given load case.

	T	BF	NO	WB	WT
T	Full	High	Low-High	Very Low	Very Low
BF	High	Full	Low-High	Very Low	Very Low
NO	Low-High	Low-High	Full	Very Low	Very Low
WB	Very Low	Very Low	Very Low	Full	Very High
WT	Very Low	Very Low	Very Low	Very High	Full

The correlations between the various load effects for a given load, as specified in Table 4, are self-explanatory. However, for those between various loads, it is considered that T, BF, and NO have higher mutual correlations relative to that with WB and WT due to their phenomenological basis in train and track geometry. The correlation of T and BF with NO is more complex and, therefore, considered to be varying between medium to high ranges. Nibloe et al. [58] noted that the proportion of lateral forces to vertical forces changes significantly at higher vehicle speeds and is significantly larger for empty trains. Therefore, the correlations between train and nosing loads can be suitably adjusted between low to high ranges to minimize the simultaneous occurrences of high vertical train and lateral nosing loads based on train speed and occupancy.

3.4.3. Isoprobabilistic transformation considerations

Due to the high reliance on engineering expert judgement for the specification of correlation values, the constructed correlation matrix can be symmetric but not necessarily positive semi-definite as is mathematically required. Physically, it indicates that at least one load's correlations can be expressed as a linear combination of the others. This situation invalidates the use of Cholesky decomposition in the standard first-order reliability method (FORM) algorithms for isoprobabilistic transformation of the random variables, i.e. the transformation of the random variables from the physical space to the reduced space. There can be two solutions to this problem which can work together.

Firstly, instead of Cholesky decomposition, the singular value decomposition (SVD) of the correlation matrix in physical space, $\mathbf{C_X}$, can be used to determine the isoprobabilistic transformation matrix based on the orthonormal eigenvectors corresponding to the eigenvalues of $\mathbf{C_X}$. The main advantage of utilizing SVD is that it imposes a symmetric positive semi-definite requirement on $\mathbf{C_X}$ as opposed to Cholesky decomposition, which imposes a positive definite requirement on $\mathbf{C_X}$.

Finally, when engineering expert judgement results in a symmetric but non-positive definite correlation matrix, its nearest positive semi-definite matrix can be determined using Higham's Nearest Correlation Matrix algorithim [59]. For example, for a case with three loads with correlations $C_{12} = 0.9$, $C_{13} = 0.1$, and $C_{23} = 0.9$, then Higham's algorithm gives modified correlation values of $\tilde{C}_{12} = 0.77$, $\tilde{C}_{13} = 0.185$, and $\tilde{C}_{23} = 0.77$. This strategy has many applications in finance but is also appropriate for structural reliability assessments. Thus, a significant constraint associated with load correlations can be remedied.

3.5. Factor adjustment challenges

3.5.1. Model uncertainty considerations

While the LSF usually includes variables other than load and resistance, such as model errors as shown in Equations (9) and (10), the design equation (Equation (7)) typically includes only load and resistance variables. Therefore, the effects of such accompanying variables must be incorporated in the consequent estimates of adjusted factors. This is done by scaling the design values of the load and resistance variables with those of load and resistance model errors before estimating the adjusted partial factors.

3.5.2. Calibrating adjusted factors

Adjusting partial factors can lead to many estimates for high-dimensional problems. The generally adopted method for adjusting factors, as discussed in Section 2.4.1, yields estimates of combination factors that vary per load case. When a structural member is assessed at n cross sections for j load cases with l loads, the total number of estimated adjusted factors is $n \times j \times l$. Ideally, there should only be l partial factors and j combination factors. This problem will be further compounded when there are be multiple structural members of the same type (e.g. two longitudinal girders for the same span with the same geometry). Therefore, obtaining an optimized set of adjusted factors is a significant problem that compounds higher dimensional problems.

A potentially quicker approach to calibrate the adjusted factors is to envelope the factor estimates based on their maximum. Such an enveloping for a structural member can be across all cross sections, load effects, and load cases under consideration, and its impact can be assessed using a design check (Section 2.4.3). Any such conservative enveloping will result in a structural design greater than the initially targeted reliability index β_T. Therefore, the primary advantage of a probabilistic assessment can be reduced with enveloped factors. However, a more targeted and thematic enveloping of factors (e.g. by enveloping factors for a particular structural member type) can minimize the efficiency lost.

4. Case study: probabilistic assessment of old steel railway truss bridge

4.1. Bridge overview

The probabilistic framework presented in Section 2 with the modelling approaches presented in Section 3 is applied and demonstrated on a case study inspired by an existing steel truss railway bridge in Australia as illustrated in Figure 2. The two longitudinal girders of the bridge, spanning 60 m in length over eight bays, are examined. The cross sections of these girders are presented in Figure 3. The cross sections at intermediate lengths between intersections with transverse girders have additional plates at the top and bottom. Each girder is analyzed at cross sections at increments of 2.5 m. Therefore, the total number of sections for reliability assessment is $2 \times 60/2.5 = 48$ sections. Considering the widespread literature on non-linear FEA modelling of steel structures [35], this case study focusses on calibrating the factors for such an assessment.

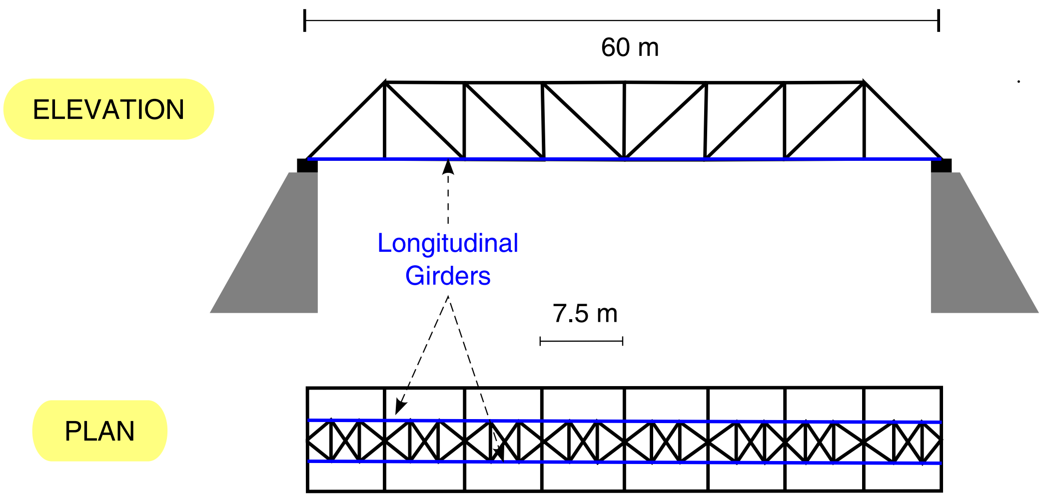

Figure 2: Illustration of the truss bridge in the case study.

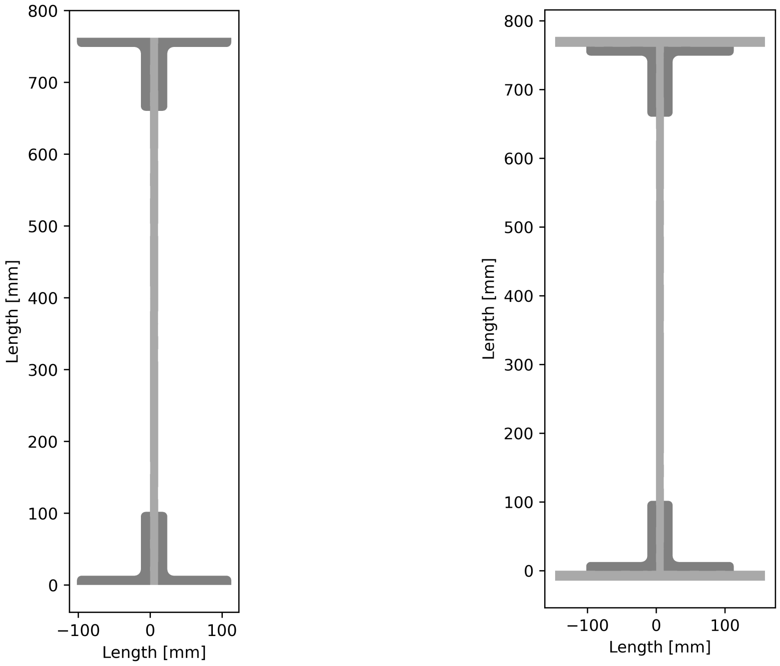

(a) Intersection

(b) Intermediate

Figure 3: Cross-sectional geometry of longitudinal girders.

4.2. Uncertainty quantification and probabilistic modelling

For ultimate limit state, the combined action of various loads is considered for the assessment: Dead Load (DL), Superimposed Dead Load (SDL), Track Load (TL), Train Load (T), Braking Force (BF), Nosing Load (NO), Wind on Bridge (WB), and Wind on Train (WT), i.e.

$$\mathcal{S} = \{\text{DL, SDL, TL, T, BF, NO, WB, WT}\} \tag{12}$$

. The statistics of the random variables are summarized in Table 6. Some essential references and considerations for establishing these statistical models are discussed earlier in Section 3.

Table 6: Statistics of random variables.

Variable	Label	Type	Nominal	Bias	CoV	Ref
Dead load	DL	Normal	varies	0.97	0.08	[60]
Superimposed dead load	SDL	Normal	varies	1.00	0.25	[60]
Track loads	TL	Normal	varies	1.00	0.25	[60]
Train load	T	Gumbel	varies	0.83	0.10	[19]
Nosing load	NO	Gumbel	varies	0.83	0.10	[19]
Braking force load	BF	Gumbel	varies	0.83	0.10	[19]
Wind on bridge	WB	Gumbel	varies	0.40	0.28	[18]
Wind on train	WT	Gumbel	varies	0.53	0.28	[18]
Resistance uncertainty	ω_R	Lognormal	1.0	1.0	0.05	[61]
Load uncertainty	ω_S	Lognormal	1.0	1.0	0.10	[61]
Yield strength [MPa]	F_y	Normal	268.5	1.0	0.031	Updated

4.2.1. Nominal load and resistance values

To determine nominal load effect values, a linear elastic analysis model of the bridge is developed using typical commercial structural analysis software. The static load effects — DL, SDL, TL, BF, WB — are directly estimated from the model whereas the transient effects — T, NO, and WT — are estimated using the influence lines developed using the model for each section to obtain their maximum value. Additionally, the nominal values of moment and axial resistance are determined as per AS 5100.6 [37] Cl. 5.2, with due consideration to section classification. The resulting complete database of nominal load effects is shared with this manuscript as a part of data availability.

4.2.2. Train load effects (S_T)

The train for assessment consists of one six-axle locomotive and three following four-axle wagons coupled at a spacing of 4.225 m, 3.45 m, and 3.45 m, with axle spacing specified in Figure 4. Based on the railway line operator specifications, each axle nominally weighs 20 t. In the absence of data regarding the distribution of axle loads, we use the results from Nowak and Rakoczy [19] for determining train load effect bias and CoV with a Gumbel distribution. Considering the 20 t as a 97.5 percentile value, and a CoV of 0.10 and a bias of 0.83 as reported by Nowak and Rakoczy [19] for bridges greater than 24 m, the statistics of the vertical train load effects are determined.

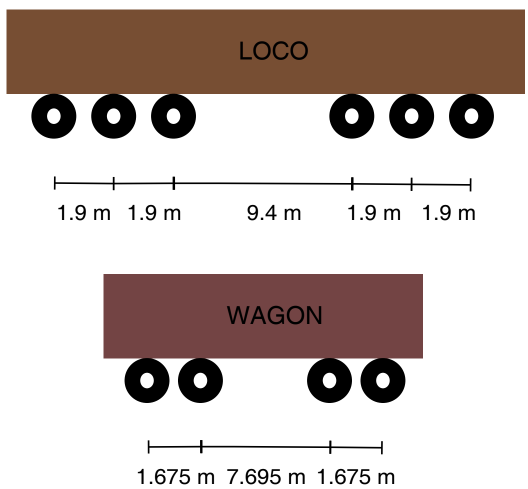

Figure 4: Locomotive and wagon axle spacing.

4.2.3. Horizontal load effects

Braking forces for structural analysis are estimated and applied as per AS 5100.2 [17] for railway structures. For the horizontal nosing force, the influence lines are developed using a unit load. The design vehicle with an axle load equal to the actual nosing load, i.e. 67 kN as per AS 5100.2 [17], is used to determine the nominal nosing load effects.

4.2.4. Annual maximum wind speed statistics

The bridge is located in the cyclonic region C as per AS-NZS 1170.2 [62] with an annual maximum wind velocity of 79 m/s, based on three-second gust data, at a return period of 2000 years as specified in AS 5100.2 [17] Cl. 17.7.2. The CoV of wind velocity is taken as 0.30 from ABCB [20] Table C.6 with a Gumbel distribution. Using the CoV and return period, the bias of wind distribution can be determined as specified in Caprani et al. [18]. The resulting distribution is presented in Figure 5. This distribution serves as an important basis for establishing the statistics of the consequent load effects: wind on the bridge (S_{WB}), and; wind on the train (S_{WT}).

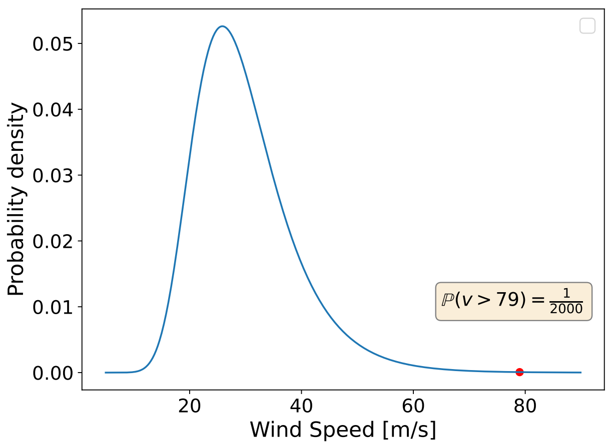

Figure 5: Distribution of annual maximum wind speed.

4.2.5. *Wind on bridge load effect (S_{WB})*

The nominal value of the transverse wind load is estimated as per AS 5100.2 [17] Cl. 17.3. for a nominal wind velocity of 79 m/s as specified in Section 4.2.4. This load is applied to the linearly elastic analysis model to estimate the nominal value of S_{WB} load effect at each section under consideration. Even though the load effect is not a linear function of wind speed, it is also considered to be of type Gumbel distribution with a bias equal to that of the wind speed. Indeed, since wind pressure, and thus load effects, are proportional to the wind speed squared, the CoV of WB, $CoV_{S_{\mathrm{WB}}}$, is estimated using CoV_v [63]:

$$CoV_{S_{\mathrm{WB}}} \approx \frac{CoV_v\sqrt{4+2CoV_v^2}}{1+CoV_v} \tag{13}$$

4.2.6. *Wind on train load effect (S_{WT})*

Influence lines for estimating the wind on train load effect are developed using a unit load acting normally to the area of an idealized rectangular train of height 4 m. The transverse wind load acting per axle of the locomotive and wagon is estimated by determining the ultimate transverse wind design loads as per AS 5100.2 [17] Cl. 17.3.1. Then, the design train with the estimated wind loads per axle is utilized to estimate the nominal values of consequent load effect S_{WT} using the influence lines. The bias of and the CoV of S_{WT} are established as that for S_{WB}, as specified in Section 4.2.5.

4.2.7. *Yield strength distribution*

The statistics of yield strength F_y are established by utilizing the in-situ measurements using Bayesian statistics. Considering a low carbon steel based on site investigations, the prior distribution of steel yield strength is taken to be normally distributed with a nominal value of 230 MPa. Using [39] recommendations, a bias of 1.05 and CoV of 0.05 is taken. Using a normally distributed likelihood with a known precision equal to the standard deviation of the measurements, i.e. $\sigma_\epsilon = \sigma_{x_i}$, the parameters of the posterior distribution of F_y can be determined using standard Bayesian updating. Figure 6 shows the prior and posterior distribution of steel yield strength along with the measurements. This posterior distribution is used in the reliability analyses.

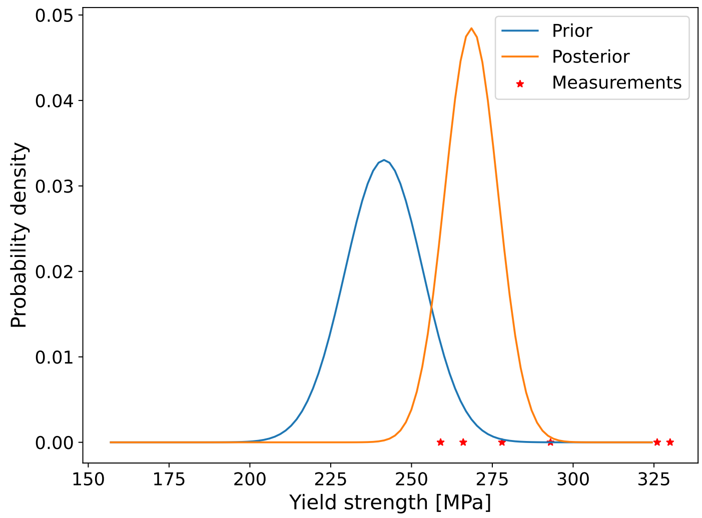

Figure 6: Prior and posterior distributions of steel yield strength.

4.2.8. Correlations

The considerations as discussed in Section 3.4.2 and table 4 are utilized to establish the correlations between various loads and load effects. The correlation between major and minor bending moments is considered to be 0.95, while the correlation between moments and the axial load effects is considered to be 0.80. Similarly, the recommendations in Table 5 are utilized to establish the correlations between the loads. The vertical train loads T are considered to be correlated with the BF and NO with a correlation coefficient of 0.70. Similarly, WB and WT are considered to be correlated with a coefficient of 0.90. All other load variable combinations are considered to be uncorrelated. Furthermore, the correlation values are modified as per Higham [59] and singular value decomposition is used for isoprobabilistic transformation of the random variables.

4.3. Reliability assessment & factor calibration

Using the probabilistic models specified in Section 4.2, a probabilistic assessment for the two longitudinal girders is conducted. Load combinations are taken as per Section 3.4.1 and table 3. After estimating the in-situ reliabilities, the partial safety factors and combination factors are adjusted and calibrated.

4.3.1. LSF

The LSF for evaluating the reliability of the girders at ULS under combined load action is:

$$g\left(\boldsymbol{X}\right) = \omega_R - \omega_S \left[\left| \frac{M_{z_S}}{z \cdot M_{z_R}} \right| + \left| \frac{M_{y_S}}{z \cdot M_{y_R}} \right| + \left| \frac{N_S}{z \cdot N_R} \right| \right] \tag{14}$$

where M_{z_S} is the total z-axis (major axis) moment for all load cases as given by,

$$\begin{aligned} M_{z_S} = & M_{z_{DL}} + M_{z_{SDL}} + M_{z_{TL}} + M_{z_T} \\ & + M_{z_{BF}} + M_{z_{NO}} + M_{z_{WB}} + C_v \ M_{z_{WT}} \end{aligned} \tag{15}$$

M_{y_S} is the total y-axis (minor axis) moment for all load cases as given by,

$$\begin{aligned} M_{y_S} = & M_{y_{DL}} + M_{y_{SDL}} + M_{y_{TL}} + M_{y_T} \\ & + M_{y_{BF}} + M_{y_{NO}} + M_{y_{WB}} + C_v \ M_{y_{WT}} \end{aligned} \tag{16}$$

N_S is the total axial force given by,

$$\begin{aligned} N_S = & N_{DL} + N_{SDL} + N_{TL} + N_T \\ & + N_{BF} + N_{NO} + N_{WB} + C_v \ N_{WT} \end{aligned} \tag{17}$$

C_v is a constant parameter accounting for railway line operator decisions at high wind velocities as discussed in the following Section 4.3.2, and z is a scalar calibration parameter for achieving β_T. For in-situ reliability estimation, $z = 1$. Also, M_{z_R} and M_{y_R} are estimated as per AS 5100.6 [37] Cl. 5.2 depending upon F_y, with due consideration to section compactness. Therefore, the LSF consists of $8 \times 3 + 3 = 27$ random variables.

Similar to Equation (14), the design equation for the design check is given as,

$$z = \left| \frac{\sum_{s \in \mathcal{S}} \gamma_s \ \psi_s \ M_{z,k_s}}{\phi \cdot M_{z_R}} \right| + \left| \frac{\sum_{s \in \mathcal{S}} \gamma_s \ \psi_s \ M_{y,k_s}}{\phi \cdot M_{y_R}} \right| + \left| \frac{\sum_{s \in \mathcal{S}} \gamma_s \ \psi_s \ N_{k_s}}{\phi \cdot N_R} \right| \tag{18}$$

where, M_{z,k_s}, M_{y,k_s}, and N_{k_s} are the nominal values of the major, minor, and axial load effects, respectively, for load s with appropriate consideration of C_v.

4.3.2. Incorporating operator decisions at $v \geq 28$ m/s

As discussed in Section 3.3.1, a threshold of $v \geq 28$ m/s is adopted. From Figure 5 we know

$$\mathbb{P}\left[v \geq 28 \text{ m/s}\right] = \frac{1}{1.92} \approx 0.52 \tag{19}$$

and so

$$\mathbb{P}\left[v < 28 \text{ m/s}\right] = 1 - \mathbb{P}\left[v \geq 28 \text{ m/s}\right] = C_v = 0.48 \tag{20}$$

Therefore, the probability of the wind on train load effect is equal to the joint probability of the load effect and the probability of wind speed $v < 28$ m/s. Consequently, assuming independence, all WT load effects in Equations (15) to (17) are multiplied with $C_v = 0.48$. Clearly more advanced models can be developed that account for the complexities of such railway-line operator decisions.

4.3.3. Safety and combination factor calibration

Using the developed reliability assessment model, adjusted and calibrated partial and combination factors can be developed for the girders as discussed in Section 2.4. The reliabilities of girders are calibrated to β_T. AS 5104 [64] Table G.4 provides guidance in selecting an appropriate annual β_T based on economic optimization. Based on inputs from the asset owner, and considering large consequences of failure with normal costs of the relative safety measures, $\beta_T = 4.4$ is taken. For calibrating the reliabilities, the nominal section resistances are calibrated via the scalar design parameter, z.

The 48 sections are calibrated for each of the 3 load cases; i.e. 144 reliability analyses are calibrated. The factors ϕ, γ, and ψ are estimated for each of the 48 girder sections. As specified in Section 2.4.1, the comparison of the coefficient approach results in unique estimates of γ for the $5 \times 3 = 15$ varying load effects at each section. In contrast, the estimates of γ for the $3 \times 3 = 9$ static load effects, ψ for the 15 varying load effects, and ϕ for the 1 resistance random variable F_y differ per load case. As discussed in Section 3.5.1, the effects of ω_R and ω_S are absorbed within the load and resistance design values. Considering all the load cases for all sections, there are $144 \times 9 + 48 \times 15 = 2016$ estimates of adjusted γ; 144×1 estimates of adjusted ϕ, and; $144 \times 15 = 2160$ estimates of adjusted ψ. Therefore, considering the large volume of data and the high dimensionality of the problem, these adjusted estimates of factors will also be calibrated and checked as discussed in Sections 2.4.2 and 2.4.3.

4.4. Results

This section presents the results from the probabilistic assessment of the two girders. The input nominal values, resulting calibrated design points, and factors for the left girder section at 30 m, L-30, are provided and discussed in Appendix A. Similar data is provided for all the 48 sections as a Zenodo repository for full reproducibility of our work [16]. Furthermore, the in-situ reliabilities and the calibrated design parameter, z, are also provided as a spreadsheet. In this section, the results and associated trends are discussed collectively for drawing conclusions.

4.4.1. In-situ reliability and calibration

Figure 7 presents the in-situ reliabilities of the girders for all the 144 reliability assessments. Considering the volume of information, the results are presented as stacked bar graphs. Therefore, the sum of the heights of each data type (colour bar) equals one. Figure 7 indicates that there's considerable variation in the reliabilities of the two girders at various sections, ranging between 4 and 7.5. Most importantly, at most sections $\beta_T = 4.4$ is exceeded. Furthermore, the reliabilities obtained in the load case C2 with NO as maximum are generally more critical that the other two load cases. This criticality is attributed to the high M_y induced by the horizontal nosing forces. Considering that the failure surface is linear in the three load effects (Equation (14)), high M_y ends up governing as the section capacity M_{y_R} is generally much lower that M_{z_R} and, therefore, load case C2 reliabilities are more critical. At some sections, the reliabilities obtained for load case C2 are less than β_T. These sections pertain to the left girder at the intersections with the transverse girders, without the additional top and bottom flange plates. For example L-30 section has an in-situ reliability index of 4.169 for the loadcase C2. The complete database of in-situ reliabilities for all sections is also shared with this manuscript. Therefore, calibrated estimates of the partial and combination factors would be useful for a more accurately estimated resistance using non-linear FEA.

Based on the probabilistic model, all 144 reliability assessments are calibrated to achieve β_T as elaborated in Section 2.4 and Figure 1. As expected, Figures 7 and 8 demonstrate an inverse relationship; i.e. higher reliabilities result in relatively lower estimates of the design parameter. For example, the

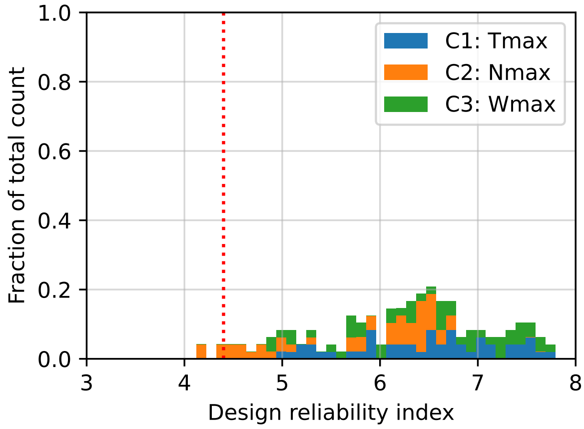

Figure 7: In-situ reliabilities of girder sections.

L-30 section has a calibrated z value equal to 1.011 for the loadcase C2. A reliability analysis with the calibrated value of the design parameter results in a reliability index equal to β_T. The design points from the reliability assessments calibrated at β_T are utilized for estimating the adjusted factors as elaborated in Section 2.4.1.

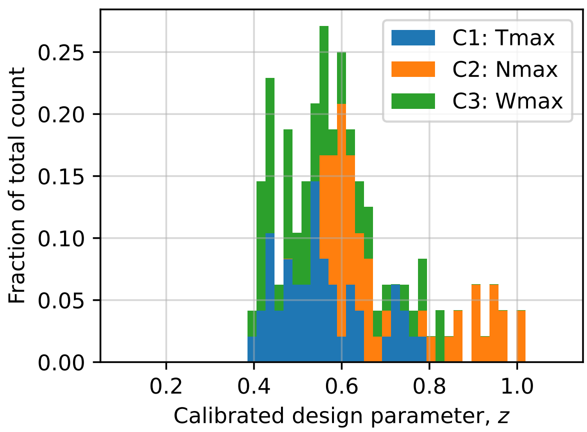

Figure 8: Calibrated design parameter, z, for various load cases.

4.4.2. *Adjusted factors*

Figure 9 presents the histograms of estimated adjusted factors. Some important statistical descriptors of these adjusted factors are presented in Table A.8. Table A.9 presents the estimated factors for section L-30 with all corresponding nominal values. The effects of ω_R and ω_S are incorporated by multiplying their design values with the appropriate load and resistance variable design point estimates as elaborated in Section 3.5.1 before estimating the adjusted factors. Note that each data type in Figure 9 contains the estimates of all three types of load effects; i.e. DL represents the factors for $M_{z_{DL}}$, $M_{y_{DL}}$, and N_{DL}, combined.

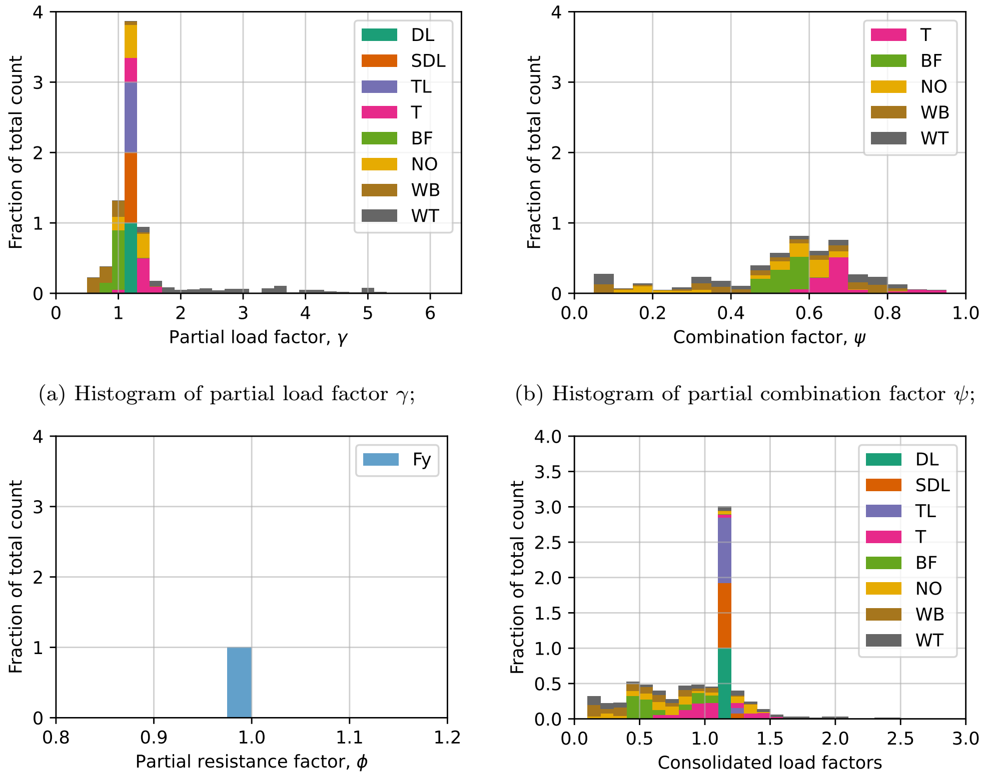

(a) Histogram of partial load factor γ;

(b) Histogram of partial combination factor ψ;

(c) Histogram of partial resistance factor ϕ;

(d) Histogram of consolidated γ and ψ.

Figure 9: Stacked histograms of adjusted partial safety and combination factors

From Figure 9a, it is evident that most of the γ estimates are between 1 and 2, with some exceptions for loads WB and WT. Especially, the estimates of the static load effects, i.e. DL, SDL, and TL, are very close to 1. The exceptions will be discussed in the following paragraphs. Likewise, Figure 9b indicates that all varying load combination factors estimates lie between 0 and 1, and Figure 9c indicates that ϕ is close to 1 for all reliability analyses. Figure 9d presents the consolidated load factors, i.e. multiplication of respective γ and ψ estimates for each reliability analyses, including C_v for WT load effects as discussed in Section 4.3.2.

As noted previously in Figure 9a, in some cases, the adjusted γ factors for load effects WB and WT exhibit different behaviour compared to the remaining γ factors. In some cases, the γ estimates for WB are less than 1. Considering that WB represents load variables, this may seem aberrational, but four important points are noteworthy. Firstly, there is no unique solution to the partial factor calibration problem. Theoretically, infinite combinations of factors can yield the same target reliability index. Secondly, the most important aspect is that the estimated factors collectively yield a design $\geq \beta_T$. This aspect will be verified in the following paragraphs. Thirdly, the partial factor estimates for structural design codes are highly rationalized for a conservative structural design for a wide variety of structures, while these adjusted factors are application for the specific girder sections under consideration and the chosen probabilistic representation of WB. Finally, a lower estimate of γ for WB most likely indicates a high conservativism in the load model for WB. Considering that cyclonic gust wind velocity of 79 m/s was considered, such an interpretation seems reasonable.

In addition to WB, WT demonstrates some varying behaviour with some very high estimates of γ for some load cases. However, this behaviour is attributed to the scalar multiplier C_v within the LSF (Equation (14)) accounting for the railway line operator decisions as discussed in Section 4.3.2. When the factors including C_v are consolidated, the resulting multiplying factors for WT are tempered as seen from Figure 9d.

4.4.3. Design efficiency

The efficacy of the adjusted partial factors can be determined using a design check as elaborated in Section 2.4.3. Figure 10 presents the resulting reliabilities from a design conducted by the adjusted factors. The multiplicity of the estimated factors and the challenges associated with their enveloping is discussed in Section 3.5.2. Considering these challenges, two possible scenarios are explored. In the first scenario, the adjusted factors, with some estimates varying per load case, for each section are rounded-off to the second decimal place and used as it is in a design check. The design reliabilities obtained as presented in Figure 10a. As most design reliabilities are very close to β_T, it demonstrates the high efficiency of the estimated factors. To evaluate the efficiency of the obtained design, the squared L2 norm with respect to β_T can be estimated as,

$$||e|| = ||\boldsymbol{\beta_d} - \mathbf{1}\beta_T|| = \sum_{i=1}^{144} (\beta_{d_i} - \beta_T)^2 \tag{21}$$

The first scenario yields design reliabilities with L2 norm of

$$||e_1|| = 0.88$$

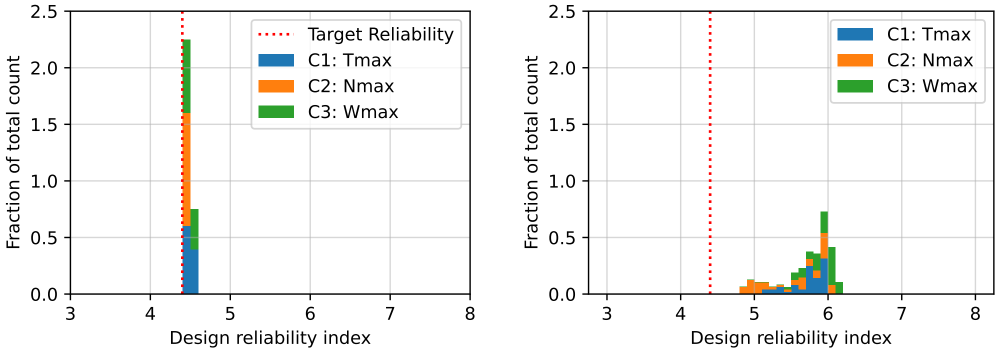

(a) Design using rounded-off adjusted factors; (b) Design using factors enveloped for maximum;

Figure 10: Design reliabilities obtained using calibrated factors.

In the second scenario, the global maximum estimate of the partial load, partial resistance, and load combination factors are taken and a design is conducted for each of the 144 reliability analyses. The results are presented in Figure 10b. Such a global maximum enveloping reduces the problem to a total of 40 factors (1 partial resistance factor, 24 partial load factors, and 15 load combination factors) from a total of 3456 factors (144×1 partial resistance factors, 2016 partial load factors, and 2160 load combination factors). It is evident from Figure 10b that the design reliabilities so obtained are significantly greater than β_T. This approach yields design reliabilities with an L2 norm of

$$||e_2|| = 16.33 \gg ||e_1||$$

Therefore, significant efficiency is lost in dimensionality reduction. These designs are summarized in Table 7.

Table 7: Comparison of design number of factors and efficiencies.

Design	γ	ψ	ϕ	Total Factors	Design L2 Norm
As is	$144 \times 9 + 48 \times 15 = 2016$	$144 \times 15 = 2160$	144	4320	0.88
Max envelope	24	15	1	40	16.33

5. Conclusions

This study presents a scalable and generalized framework for the probabilistic assessment of steel railway bridges using adjusted partial and combination factors, focused on the Ultimate Limit State. The proposed framework is composed of four sequential stages: (i) initial analysis and database generation; (ii) uncertainty quantification; (iii) adjustment and calibration of factors, and; (iv) final performance check. These four stages utilize six mutually cooperating analysis modules for: (i) structural properties; (ii) linear elastic analysis; (iii) reliability analysis; (iv) Bayesian data assimilation; (v) factor adjustment, and; (vi) non-linear analysis. Several challenges associated with the probabilistic modelling and assessment for steel railway truss bridges are discussed and some solutions are proposed in the study. These challenges related to: (i) load effect and resistance uncertainties; (ii) horizontal forces such as braking and nosing; (iii) wind loads and railway line operator decisions; (iv) load effect combinations and correlations, and; (v) partial and combination factor adjustment. The scarce data availability and statistical models, particularly for horizontal loads, are noted for future research.

The framework is demonstrated for the assessment of two longitudinal girders of a single 60 m span steel truss bridge. The two girders are assessed at increments of 2.5 m along the length. The results indicate that the horizontal nosing forces are critical for the girder sections, with some sections yielding an in-situ reliability index less than the target reliability. The adjusted partial factors are generally found to be within 1 and 2. Likewise, the adjusted load combination factors are generally found to be between 0 and 1. A design check is conducted to evaluate the efficacy of the adjusted factors using two different strategies. It is found that there is a significant loss of design efficiency with a global maximum enveloping of factors. It is found that a 108-fold reduction in number of factor estimates with a global maximum enveloping of partial factors results in approximately 18-fold loss of design efficiency. Future work will focus on developing more efficient methods of problem dimensionality reduction and on quantifying the potential monetary benefit of such a probabilistic assessment.

Appendix A. Calibration results

Table A.8 presents the summarized statistics of the partial load and combination factors. The estimates are discussed in Section 4.4.2. The maximum values are used in the maximum design as discussed in Section 4.4.3.

Table A.9 presents the calibration results for the section L-30; where X_k represents the nominal value and X^* represents the calibrated design point. The nominal values for the moment and axial load effects are given in kNm and kN, respectively. The calibrated design point values correspond to the value of the load effect at the calibrated z for each loadcase. Using

Table A.8: Summarized statistics of partial load factor γ and combination factor ψ.

Load Effect	Partial Load Factor				Load Combination Factor			
	μ_γ	σ_γ	γ_{max}	γ_{min}	μ_ψ	σ_ψ	ψ_{max}	ψ_{min}
$M_{z_{DL}}$	1.14	0.02	1.17	1.11	—	—	—	—
$M_{y_{DL}}$	1.14	0.02	1.17	1.11	—	—	—	—
N_{DL}	1.14	0.01	1.17	1.11	—	—	—	—
$M_{z_{SDL}}$	1.18	0.02	1.2	1.13	—	—	—	—
$M_{y_{SDL}}$	1.17	0.02	1.2	1.13	—	—	—	—
N_{SDL}	1.17	0.02	1.19	1.13	—	—	—	—
$M_{z_{TL}}$	1.18	0.02	1.2	1.13	—	—	—	—
$M_{y_{TL}}$	1.17	0.02	1.2	1.13	—	—	—	—
N_{TL}	1.17	0.02	1.19	1.13	—	—	—	—
M_{z_T}	1.34	0.14	1.57	1.05	0.69	0.08	0.94	0.58
M_{y_T}	1.34	0.14	1.57	1.05	0.69	0.08	0.94	0.58
N_T	1.31	0.13	1.5	1.05	0.68	0.08	0.91	0.58
$M_{z_{BF}}$	0.95	0.06	1.08	0.87	0.52	0.03	0.59	0.48
$M_{y_{BF}}$	0.96	0.06	1.09	0.87	0.53	0.03	0.59	0.49
N_{BF}	0.98	0.06	1.09	0.88	0.54	0.03	0.59	0.48
$M_{z_{NO}}$	1.25	0.12	1.38	0.94	0.49	0.18	0.67	0.15
$M_{y_{NO}}$	1.27	0.13	1.4	0.95	0.5	0.18	0.68	0.15
N_{NO}	1.16	0.1	1.29	0.92	0.45	0.18	0.63	0.12
$M_{z_{WB}}$	0.71	0.24	1.12	0.33	0.48	0.23	0.81	0.07
$M_{y_{WB}}$	0.7	0.24	1.11	0.33	0.48	0.23	0.82	0.07
N_{WB}	0.79	0.32	1.37	0.33	0.49	0.25	0.84	0.05
$M_{z_{WT}}$	3.08	1.19	5.22	1.32	0.49	0.24	0.83	0.06
$M_{y_{WT}}$	3.11	1.21	5.32	1.32	0.49	0.24	0.84	0.06
N_{WT}	2.78	0.97	4.45	1.28	0.48	0.23	0.81	0.07

these design point values, the partial load and combination factors can be estimated as elaborated in Section 2.4. For the time invariant load effects we obtain load factors that vary per load case. For example, for load effect $M_{z_{DL}}$, the load factors are given by,

$$\begin{aligned} \tfrac{9.78\times1.14}{10.06} &= 1.11 \\ \tfrac{9.78\times1.18}{10.06} &= 1.15 \\ \tfrac{9.78\times1.15}{10.06} &= 1.12 \end{aligned} \tag{A.1}$$

Similarly, for time variant laod effects, such as M_{z_T}, the partial load factors are obtained by,

$$\begin{aligned} \tfrac{187.37\times1.14}{160.43} &= 1.33 \\ \tfrac{187.37\times1.18}{160.43} &= 1.38 \\ \tfrac{187.37\times1.15}{160.43} &= 1.34 \end{aligned} \tag{A.2}$$

Considering the estimate for the dominating load case (C1) as the unique partial factor estimate, i.e. 1.33, the load combination factors can be determined as,

$$\begin{aligned} \tfrac{121.86}{187.37} &= 0.65 \\ \tfrac{124.14}{187.37} &= 0.66 \end{aligned} \tag{A.3}$$

Similar data is provided for all 48 sections as a spreadsheet for ease of reproducibility [16].

References

[1] ASCE, 2021 report card for America's infrastructure, American Society of Civil Engineers, Reston, VA, 2021.

[2] J. Bień, L. Elfgren, J. Olofsson (Eds.), Sustainable bridges: assessment for future traffic demands and longer lives, Dolnośląskie Wydawnictwo Edukacyjne, Wrocław, Poland, 2007.

Table A.9: Calibration data with nominal values for the left girder section at 30 m, L-30, for various load combinations.

Load Effect	X_k [kNm or kN]	X* C1	X* C2	X* C3	γ or ϕ C1	γ or ϕ C2	γ or ϕ C3	ψ C1	ψ C2	ψ C3
$M_{z_{DL}}$	10.06	9.78	9.78	9.78	1.11	1.15	1.12	1	1	1
$M_{y_{DL}}$	0.01	0.01	0.01	0.01	1.11	1.15	1.12	1	1	1
N_{DL}	-4.54	-4.4	-4.4	-4.4	1.11	1.14	1.11	1	1	1
$M_{z_{SDL}}$	2.74	2.74	2.74	2.74	1.14	1.18	1.15	1	1	1
$M_{y_{SDL}}$	0	0	0	0	1.14	1.18	1.15	1	1	1
N_{SDL}	-0.24	-0.24	-0.24	-0.24	1.14	1.18	1.15	1	1	1
$M_{z_{TL}}$	3.81	3.83	3.83	3.83	1.15	1.18	1.15	1	1	1
$M_{y_{TL}}$	0	0	0	0	1.15	1.18	1.15	1	1	1
N_{TL}	-0.34	-0.34	-0.34	-0.34	1.14	1.18	1.15	1	1	1
M_{z_T}	160.43	187.37	121.86	124.14	1.33	1.38	1.34	1	0.65	0.66
M_{y_T}	0.02	0.03	0.02	0.02	1.33	1.38	1.34	1	0.65	0.66
N_T	8.8	10.07	6.49	6.61	1.31	1.35	1.32	1	0.64	0.66
$M_{z_{BF}}$	0.51	0.44	0.24	0.24	0.98	1.01	0.98	1	0.55	0.55
$M_{y_{BF}}$	0	0	0	0	0.89	0.92	0.9	1	0.51	0.51
N_{BF}	9.06	7.77	4.28	4.29	0.98	1.01	0.98	1	0.55	0.55
$M_{z_{NO}}$	41.38	25.53	41.8	24.71	1.15	1.19	1.16	0.61	1	0.59
$M_{y_{NO}}$	32.89	20.88	33.76	20.2	1.17	1.21	1.18	0.62	1	0.6
N_{NO}	535.18	291.42	505.34	282.29	1.08	1.11	1.08	0.58	1	0.56
$M_{z_{WB}}$	-0.91	-0.3	-0.29	-0.5	0.63	0.65	0.64	0.6	0.58	1
$M_{y_{WB}}$	-5.55	-1.82	-1.76	-3.05	0.63	0.65	0.63	0.59	0.58	1
N_{WB}	972.37	366.01	355.02	594.78	0.7	0.72	0.7	0.62	0.6	1
$M_{z_{WT}}$	39.29	56.65	54.98	92.71	2.69	2.78	2.71	0.61	0.59	1
$M_{y_{WT}}$	7.08	10.32	10.02	16.9	2.72	2.81	2.74	0.61	0.59	1
N_{WT}	107.91	144.18	140.07	240.27	2.54	2.63	2.56	0.6	0.58	1
ω_S	1	1.14	1.18	1.15	0	0	0	0	0	0
F_y	254.98	265	264.13	264.83	0.99	0.99	0.99	0	0	0
ω_R	1	0.97	0.96	0.96	0	0	0	0	0	0

[3] AASHTO MBE-3, Manual for Bridge Evaluation, third ed., American Association of State Highway and Transportation Officials (AASHTO), Washington, D.C., United States, 2018.

[4] AS 5100.7, Bridge design – Part 7: Bridge assessment, Standards Australia, Sydney, Australia, 2017.

[5] M. Sýkora, M. Holický, J. Marková, Verification of existing reinforced concrete bridges using the semi-probabilistic approach, Engineering Structures 56 (2013) 1419–1426. doi:10.1016/j.engstruct.2013.07.015.

[6] R. Caspeele, M. Sykora, D. L. Allaix, R. Steenbergen, The design value method and adjusted partial factor approach for existing structures, Structural Engineering International 23 (2013) 386–393. doi:10.2749/101686613X13627347100194.

[7] M. S. Khan, C. Caprani, S. Ghosh, J. Ghosh, Value of strain-based structural health monitoring as decision support for heavy load access to bridges, Structure and Infrastructure Engineering 18 (2022) 521–536. doi:10.1080/15732479.2021.1890140.

[8] V. Nadolski, M. Holický, M. Sýkora, Comparison of approaches to reliability verification of existing steel railway bridges, Section Building Structures & Structural Mechanics 21 (2021). doi:10.35181/tces-2021-0015.

[9] J. R. Casas, C. Cremona, G. Holm, R. Karoumi, C. Melbourne, M. Plos, M. Sloth, D. Wisniewski, K. Gylltoft, S. Thelandersson, B. Johansson,

L. Elfgren, Guideline for Load and Resistance Assessment of Existing European Railway Bridges : Advices on the use of advanced methods, Sixth Framework Programme, 2007.

[10] A. M. Rakoczy, A. S. Nowak, S. Dick, Fatigue reliability model for steel railway bridges, Structure and Infrastructure Engineering 12 (2016) 1602–1613. doi:10.1080/15732479.2016.1153664.

[11] K. A. Flanigan, J. P. Lynch, M. Ettouney, Probabilistic fatigue assessment of monitored railroad bridge components using long-term response data in a reliability framework, Structural Health Monitoring 19 (2020) 2122–2142. doi:10.1177/1475921720915712.

[12] R. Wang, J. Leander, R. Karoumi, Fatigue reliability assessment of steel bridges considering spatial correlation in system evaluation, Structure and Infrastructure Engineering 19 (2023) 254–268. doi:10.1080/15732479.2021.1938614.

[13] A. O'Connor, C. Pedersen, L. Gustavsson, I. Enevoldsen, Probability-based assessment and optimised maintenance management of a large riveted truss railway bridge, Structural Engineering International 19 (2009) 375–382. doi:10.2749/101686609789847136.

[14] J. Žitný, P. Ryjáček, M. Sýkora, S. Pospisil, S. Hracov, Probabilistic assessment of equilibrium of steel railway bridge based on wind tunnel testing, traffic and wind speed records — case study (under review), Structural Engineering International - Journal of IABSE (2023).

[15] V. N. Moreira, J. Fernandes, J. C. Matos, D. V. Oliveira, Reliability-based assessment of existing masonry arch railway bridges, Construction and Building Materials 115 (2016) 544–554. doi:10.1016/j.conbuildmat.2016.04.030.

[16] M. S. Khan, C. Caprani, R. Lenner, M. Sýkora, Dataset for reliability assessment of steel truss railway bridges at ultimate limit state under combined loads, 2023. doi:10.5281/zenodo.10042621.

[17] AS 5100.2, Bridge design – Part 2: Design Loads, Standards Australia, Sydney, Australia, 2017.

[18] C. C. Caprani, M. M. Melhem, K. Siamphukdee, Reliability analysis of a Super-T prestressed concrete girder at serviceability limit state to AS 5100:2017, Australian Journal of Structural Engineering 18 (2017) 60–72. doi:10.1080/13287982.2017.1332843.

[19] A. S. Nowak, A. M. Rakoczy, Development of System Reliability Models for Railway Bridges, Technical Report 25-1121-0001-426, Mid-America Transportation Center, Lincoln, NE, 2012.

[20] ABCB, Handbook: Structural Reliability Verification Method, Technical Report, Australian Building Codes Board, 2019.

[21] JCSS, Probabilistic Model Code, Joint Committee on Structural Safety, 2001. Jcss-ostl/dia/vrou -10-11-2000.

[22] E. T. Jaynes, Probability Theory: The Logic of Science, Cambridge University Press, 2003. doi:10.1017/CBO9780511790423.

[23] M. S. Khan, S. Ghosh, C. Caprani, J. Ghosh, Sensitivity of value of information to model and measurement errors, ASCE-ASME Journal of Risk and Uncertainty in Engineering Systems 6 (2020) 1–13. doi:10.1061/AJRUA6.0001086.

[24] R. Rackwitz, On the combination of non-stationary rectangular wave renewal processes, Structural Safety 13 (1993) 21–28. doi:10.1016/0167-4730(93)90045-3.

[25] M. Holicky, T. Vrouwenvelder, Time variant reliability of a reinforced concrete column, in: Advances in Safety and Reliability, Elsevier Science, 1997, pp. 1307–1314.

[26] R. Rackwitz, Computational techniques in stationary and non-stationary load combination-a review and some extensions, Journal of Structural Engineering 25 (1998) 1–20.

[27] R. Rackwitz, M. Holicky, Time variant reliability of a column under variable loads with intermittencies, in: Safety and reliability, AA Balkema/Rotterdam/Brookfield, 1998, pp. 977–984.

[28] C. J. Turkstra, H. O. Madsen, Load combinations in codified structural design, Journal of the Structural Division 106 (1980) 2527–2543. doi:10.1061/JSDEAG.0005599.

[29] M. Sýkora, M. Holick, Comparison of load combination models for probabilistic calibrations, in: Applications of Statistics and Probability in Civil Engineering, 2011, pp. 977–985. doi:10.1201/b11332-147.

[30] E. Castillo, Extreme Value Theory in Engineering, Elsevier Science, Saint Louis, 1988.

[31] J. D. Sørensen, Calibration of partial safety factors in danish structural codes, in: JCSS Workshop on Reliability Based Code Calibration, 2002, p. 9.

[32] C. Caprani, M. S. Khan, Determination of load combination factors for the assessment of existing bridges, in: 14th International Conference on Applications of Statistics and Probability in Civil Engineering (ICASP14), Trinity College Dublin, Dublin, Ireland, 2023, pp. 1–8.

[33] V. Nadolski, Á. Rózsás, M. Sýkora, Calibrating partial factors – methodology, input data and case study of steel structures, Periodica Polytechnica Civil Engineering (2019). doi:10.3311/PPci.12822.

[34] A. Der Kiureghian, O. Ditlevsen, Aleatory or epistemic? Does it matter?, Structural Safety 31 (2009) 105–112.

[35] EN 1993 1-1, Eurocode 3: Design of steel structures - Part 1-1: General structural rules, volume Part 1.1, European Committee for Standardization, Brussels, Belgium, 2001.

[36] AS 4100, Steel structures, Standards Australia, Sydney, Australia, 2020.

[37] AS 5100.6, Bridge design – Part 6: Steel and Composite construction, Standards Australia, Sydney, Australia, 2017.

[38] L. Cajot, Y. Conan, M. Haller, Probabilistic quantification of safety of a steel structure highlighting the potential of steel versus other materials,

EUR 21695, Directorate-General for Research, European Communities, Luxembourg, 2005.

[39] JCSS, Probabilistic Model Code – Part 3, Joint Committee on Structural Safety, 2001. Jcss-ostl/dia/vrou -10-11-2000.

[40] T. Braml, M. Keuser, A. Fischer, J. Schnell, Beurteilung der zuverlässigkeit von bestandstragwerken hinsichtlich einer querkraftbeanspruchung, Beton- und Stahlbetonbau 104 (2009) 798–812. doi:https://doi.org/10.1002/best.200900050.

[41] M. Faber, On the treatment of uncertainties and probabilities in engineering decision analysis, Journal of Offshore Mechanics and Arctic Engineering 127 (2005) 243–248.

[42] M. Hansen, Zur Auswirkung von Überwachungsmaßnahmen auf die Zuverlässigkeit von Betonbauteilen, Ph.D. thesis, 2004.

[43] C. V. Scholten, I. Enevoldsen, T. Arnbjerg-Nielsen, Reliability-based classification of the load carrying capacity of existing bridges, 291, Road Directorate, Ministry of Transport, Denmark, 2004.

[44] G. James, Analysis of traffic load effects an railway bridges, Ph.D. thesis, KTH, Civil and Architectural Engineering, 2003. NR 20140805.

[45] R. Steenbergen, A. Vrouwenvelder, Safety philosophy for existing structures and partial factors for traffic loads on bridges, Heron 55 (2010) 123 – 140.

[46] R. Greiner, J. Lindner, Interaction formulae for members subjected to bending and axial compression in eurocode 3—the method 2 approach, Journal of Constructional Steel Research 62 (2006) 757–770. doi:10.1016/j.jcsr.2005.11.018.

[47] V. Nadolski, M. Sýkora, Model uncertainties in resistances of steel members, in: Proceedings of ESREL 2015, Zurich, Switzerland, 2015, pp. 4189–4195.

[48] J. Žitný, P. Ryjáček, Reserves in load capacity assessment of existing bridges, IOP Conference Series: Materials Science and Engineering 236 (2017) 012061. doi:10.1088/1757-899X/236/1/012061.

[49] J. Kašpárek, Pravděpodobnostní hodnocení interakce mostu a koleje (Probabilistic assessment of the track-bridge interaction), Ph.D. thesis, Czech Technical University, Prague, Czech Republic, 2021.

[50] EN 1991-2, Eurocode 1: Actions on structures - Part 2: Traffic loads on bridges, European Committee for Standardization, Brussels, Belgium, 2003.

[51] AS 7508, Track Forces and Stresses, Rail Industry Safety and Standards Board, Kingston, A.C.T., Australia, 2017.

[52] UIC Code: 776-1, Loads to be considered in railway bridge design, fifth ed., International Union of Railways, 2006.

[53] L. Georgiev, L. Zdravkov, V. Tanev, M. Lepoev, Equivalent nosing force for a steel railway bridge based on in situ measurements, in: IABSE

Congress Ghent 2021 - Structural Engineering for Future Societal Needs, Ghent, Belgium, 2021, pp. 1273–1279. doi:10.2749/ghent.2021.1273.

[54] AS 7508.1, Railway Rolling Stock Track Forces and Stresses — Part 1: Locomotive Rolling Stock, Rail Industry Safety and Standards Board, Kingston, A.C.T., Australia, 2009.

[55] Deutsche Bahn AG, Richtlinie 807.04 Bautechnik, Leit-, Signal- und Telekommunikationstechnik. Ausgewählte Maßnahmen und Anforderungen and das Gesamtsystem Fahrweg/Fahrzeug–Aerodynamik/Seitenwind (in German, Structural engineering, control, signalling and telecommunications technology: Selected measures and requirements for overall track system, vehicle: Aerodynamics/ Crosswind), DB Netz AG, Frankfurt aM, 2006.

[56] T. Fujii, T. Maeda, H. Ishida, T. Imai, K. Tanemoto, M. Suzuki, Wind-induced accidents of train/vehicles and their measures in japan., Quarterly Report of RTRI 40 (1999) 50–55. doi:10.2219/rtriqr.40.50.

[57] BS EN 1990, Eurocode: Basis of structural design, British Standards Institution, 2010.

[58] I. M. Nibloe, D. Ferris, M. D. O'Rourke, An overview of railways of australia vehiclel track research and potential productivity improvements, in: Conference on Railway Engineering, Perth, Australia, 1987, pp. 35–40.

[59] N. J. Higham, Computing the nearest correlation matrix—a problem

from finance, IMA Journal of Numerical Analysis 22 (2002) 329–343. doi:10.1093/imanum/22.3.329.

[60] A. Rakoczy, A. Nowak, Reliability-based sensitivity analysis for prestressed concrete girder bridges, PCI Journal 58 (2013) 81–92.

[61] JCSS, Probabilistic Model Code – Part 2, Joint Committee on Structural Safety, 2001. Jcss-ostl/dia/vrou -10-11-2000.

[62] AS-NZS 1170.2, AS-NZS 1170-2: Structural Design Actions - Part 2: Wind Actions, 2011.

[63] E. B. Haugen, Probabilistic Approaches to Design, Wiley, London, 1968.

[64] AS 5104, General principles on reliability for structures, Standards Australia, Sydney, Australia, 2017.